Synthesis, characterization and phase transitions of the inorganic–organic layered perovskite-type hybrids $[(C_nH_{2n+1}NH_3)_2PbI_4]$ (n = 12, 14, 16 and 18)†

David G. Billing* and Andreas Lemmerer

Received (in Montpellier, France) 2nd April 2008, Accepted 27th June 2008
First published as an Advance Article on the web 1st August 2008
DOI: 10.1039/b805417g

The room temperature single-crystal structures of the inorganic–organic layered perovskite-type hybrids of general formula $[(C_nH_{2n+1}NH_3)_2PbI_4]$ (n = 12, 14, 16 and 18) have been determined. The four compounds each display two reversible phase transitions above room temperature, with phases labelled **III**, **II** and **I**. The single-crystal structures of phase **II** have also been determined. The phase transition from phase **III** to phase **II** is a first-order transition and corresponds to a change in the conformation of the alkylammonium chains and a shift of the inorganic layers relative to each other. The phase change from **III** to **II** is thermochromic for all compounds, going from a yellow to an orange colour.

Introduction

Two-dimensional hybrids, $[(C_nH_{2n+1}NH_3)_2MX_4]$ (abbreviated as C_nMX), where M is a divalent metal and X is a halogen, have been the subject of many investigations since they show a variety of structural transitions with changes in temperature. The general structure of these inorganic–organic layered perovskite-type hybrids consists of layers of corner-sharing MX_6 octahedra alternating with layers of n-$C_nH_{2n+1}NH_3$ cations. The NH_3 ammonium groups are linked to the inorganic layers by three charge assisted N–H$\cdots X$ hydrogen bonds.[1] Van der Waals forces between the alkylammonium chains exist in the organic layers. The hydrocarbon chains can be either interdigitated or non-interdigitated and tilted at various angles and directions relative to the inorganic layers. The packing of the chains is often metal dependant, as in $C_{10}CdCl$, where the non-interdigitated chains on opposite sides of the $[CdCl_4]^{2-}$ layers are tilted at $+40°$ and $-40°$ relative to the inorganic layers in the compound's lowest temperature phase.[2] This type of packing is not seen in the analogues compounds $C_{10}MnCl$[3] and $C_{10}CuCl$,[4] where the chains are all parallel in one direction, tilted at approximately $+40°$. Interdigitated chains are seen in the compounds that offer the largest separation between neighbouring metal atoms in adjacent corner-shared octahedra and have long chain lengths, as in C_9PbI,[5] which has a separation of 8.708(1) and 9.034(1) Å. In $C_{10}MnCl$[3] for example, the separation is only 7.213(8) and 7.337(2) Å. The compounds with alkylammonium cations undergo single or multiple phase transitions. The nature of the transitions depend on the length and the conformation of the alkylammonium chains. These temperature dependent phase transitions have been investigated using DSC and DTA techniques, predominantly on the compounds $[(C_nH_{2n+1}NH_3)_2MX_4]$ (n = 8–18, M = Mn, Hg and Cu; X = Br and Cl).[6]

The most comprehensive investigation *via* single crystal diffraction was performed on the compound $[(C_{10}H_{21}NH_3)_2CdCl_4]$.[2] The compound undergoes two phase transitions. The first one, at 308 K, is a displacive phase transition, and the second one, at 312 K, is a complete melting of the alkylammonium chain. These two types of phase transitions are characteristic for other long chain layered perovskite-type hybrids. The displacive phase transition is a minor transition that comes about from conformational changes within the alkylammonium chains, where the torsion angles around the N–C or C–C bonds change from *trans* to *gauche* or *vice versa* as the temperature increases. The enthalpy for this phase transition is less than that for the second phase transition, where the alkylammonium chains can show dynamical disorder along their longitudinal axis, leading ultimately to a 'quasi-melting' of the hydrocarbon part. This transition is usually the major transition. The sequence of the two phase transitions depends on the identity of the metal and the length of the chain.

The hybrids $[(C_nH_{2n+1}NH_3)PbI_4]$ undergo two phase transitions: the first phase transition is in the range from 235 K to 275 K for n = 7, 8, 9, 10,[7] and the second transition in the range from 313 to 340 K.[8] The compounds with n = 12, 16 and 18 show both phase transitions above room temperature, in the range 318 to 373 K.[9] These phase transitions are first order and arise from changes in thermal motion of the alkylammonium chains situated between the layers. The alkyl chains at room temperature are non-interdigitated and tilted at 55° to the inorganic layers[10] and are in a planar, all-*trans* conformation (see Fig. 1).[11] The chains are more ordered below the transition and as they become more disordered, a resultant change in symmetry is observed. The interlayer spacing between the layers increases with temperature as the rotational disordering increases (see Fig. 1).[9] The phase

Molecular Sciences Institute, School of Chemistry, University of the Witwatersrand, Johannesburg, PO WITS 2050, South Africa. E-mail: dave.billing@wits.ac.za; Fax: 27 11 717 6749; Tel: 27 11 717 6759
† CCDC reference numbers 692951–692958. For crystallographic data in CIF or other electronic format see DOI: 10.1039/b805417g

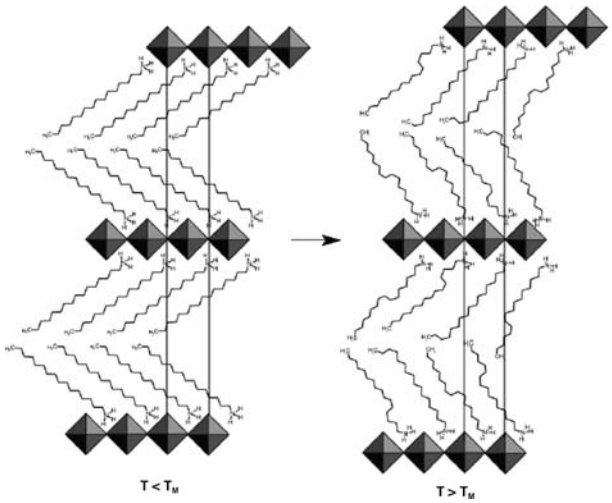

Fig. 1 Schematic depiction of the melting transition in the $[(C_nH_{2n+1}NH_3)_2PbI_4]$ hybrids studied. Reprinted with permission from Barman.[9] Copyright (2003) American Chemical Society. The structure on the left is of the room temperature phase in which the alkylammonium chains are tilted at a fixed angle and have an all-*trans* conformation. The chains are non-interdigitated and this feature is the major discrepancy between the structures reported in this study and by Barman.

transitions of these lead iodide layered perovskite-type hybrids have not been studied by single-crystal diffraction, but rather by powder diffraction, IR, NMR and Raman techniques. The objectives of this present study is determine the packing arrangement of the long chain layered perovskite-type hybrids with lead iodide at room temperature by single-crystal X-ray diffraction (SCXRD), to observe their phase behaviour using differential scanning calorimetry and to determine the single-crystal structures of the higher temperature phases.

Results and discussion

Thermal studies of $[(C_nH_{2n+1}NH_3)_2PbI_4]$ (n = 12, 14, 16 and 18) by differential scanning calorimetry and hot stage microscopy

Differential scanning calorimetry (DSC) traces were recorded for all four compounds to determine the temperature and enthalpies associated with each transition (Table 1). The samples were first cooled to 223 K to confirm that all phase transitions occur above 298 K. This is further confirmed, in our experience, by the yellow colour of the crystals at room temperature as the first phase transitions always leads to a change in colour to orange or red (See Fig. 2). The samples were then heated to a temperature above the last transition to ensure completeness and then cooled back to 298 K to illustrate the reversibility of the phase transitions (See Fig. 3). On heating, there are two endotherms, a minor one preceding a major one, which shall be referred to as the premelting, T_1, and melting transitions, T_m, respectively, consistent with the designations of Barman *et al.*[9] Both the premelting and the melting transitions are observed as exotherms upon cooling, with signs of thermal hysteresis as they occur at a lower temperature than their corresponding endotherms. The reversibility of both transitions for n = 12, 16 and 18 compounds was not observed in the study by Barman *et al.*[9] This could relate to why the structures of our compounds might be different to the proposed room-temperature structure model proposed by Venkataraman *et al.*[11] According to Barman *et al.*, only the melting transition shows an exotherm on cooling and the premelting endotherm is only recovered after leaving the samples standing for a few

Table 1 Differential scanning calorimetry results for all compounds

Chain length	T_1/°C (K)	ΔH_1/ kJ mol^{-1}	T_m/°C (K)	ΔH_m/ kJ mol^{-1}
n = 12				
Heating	41.7 (314.9)	10.9	76.5 (349.7)	44.2
Cooling	32.9 (306.1)	9.2	72.0 (345.1)	41.9
n = 14				
Heating	55.5 (328.6)	10.6	87.0 (360.1)	54.6
Cooling	47.8 (320.9)	9.6	78.8 (352.0)	51.7
n = 16				
Heating	66.9 (340.0)	11.6	95.0 (369.1)	62.7
Cooling	59.3 (332.4)	10.0	90.0 (363.2)	61.7
n = 18				
Heating	73.1 (346.3)	13.4	100.2 (373.3)	79.5
Cooling	67.6 (340.8)	12.1	93.3 (366.4)	75.9

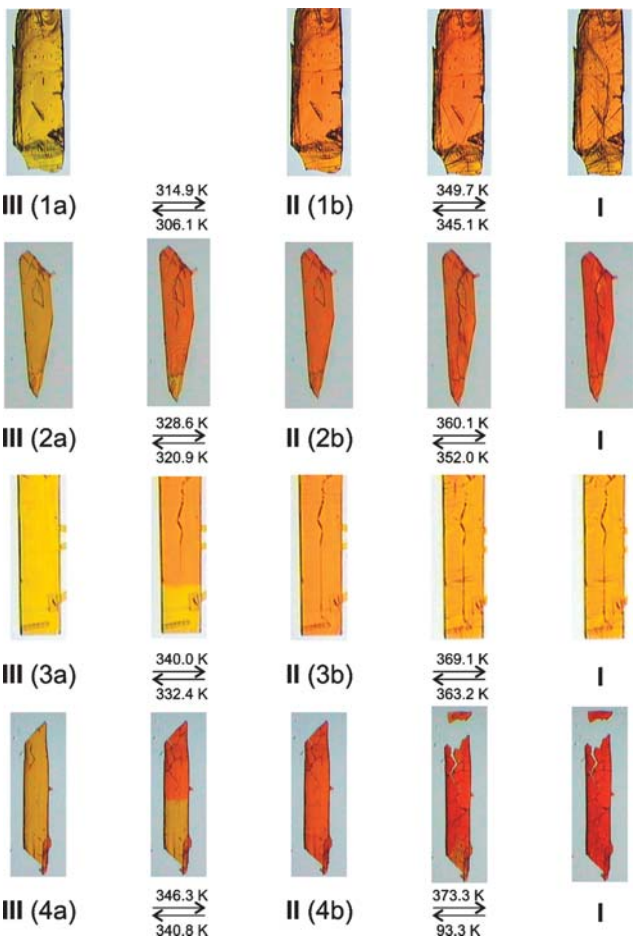

Fig. 2 Hot stage microscope pictures of crystals of the four hybrids. The crystals are yellow at room temperature, phase **III**, and then darken through orange to red in their high temperature phases, **II** and **I**.

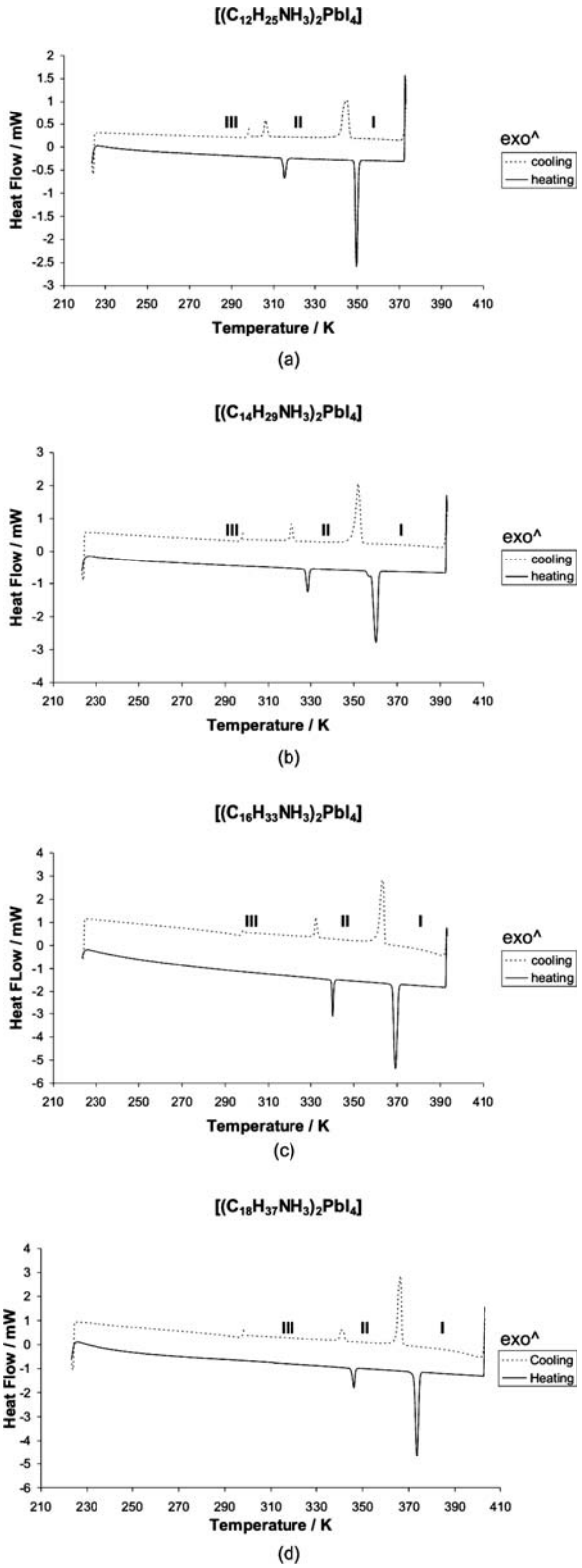

Fig. 3 Differential scanning calorimetric scans of the four layered perovskite-type hybrids. The vertical lines at either end of the scans are due to the change in the direction of the scan.

days and repeating the scan then. The enthalpies reported by Barman *et al.* are similar to our results, as shown in Fig. 4. Particularly, all the premelting transitions have similar enthalpies. This is consistent with our single-crystal structures, which indicate that the structures undergo similar geometric rearrangements at those temperatures. The melting transition enthalpies are much larger in magnitude and increase with chain length. Every compound that was heated on the diffractometer to above the melting transition temperature showed a distinct loss of crystallinity and significant fracturing of the crystals, which prevented crystallographic characterisations at these temperatures.

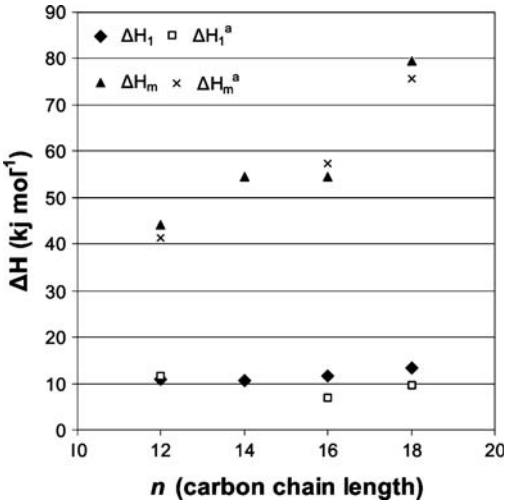

Fig. 4 Comparison of enthalpies determined in this report, shown as filled black triangles and diamonds, and those reported by Barman *et al.*[9] for C_{12}PbI, C_{16}PbI and C_{18}PbI, shown as crosses and open squares. Barman *et al.* did not report any values for C_{14}PbI.

Detailed structural consideration of the transformation of $[(C_{16}H_{33}NH_3)_2PbI_4]$

The compound $[(C_{16}H_{33}NH_3)_2PbI_4]$, abbreviated C_{16}PbI, is discussed in detail as the features of its premelting phase transition, when separated into the inorganic and organic components, can be applied to C_{12}PbI and C_{18}PbI (only the inorganic component of C_{14}PbI behaves similarly). Also in the case of C_{16}PbI, the phase transitions were observed using only one crystal, whereas two crystals each were used for C_{12}PbI and C_{18}PbI. A SCXRD dataset was collected of phase **III** at 293 K and a second one of phase **II** at 341 K. Fig. 2 clearly shows the colour change from yellow to orange that is associated with the premelting transition.

The most apparent differences between the two phases for all compounds are the crystal system, unit cell dimensions and space group. Phase **III** has an orthorhombic unit cell (*Pbca*), designated the orthorhombic phase, that contains three occupied inorganic layers at the integral values $z = 0$, 0.5 and 1. Phase **II** has a monoclinic unit cell ($P2_1/a$), designated the monoclinic phase, that contains two inorganic layers at $z = 0$ and 1. The unit cell has halved as a consequence. This behaviour is novel and not seen in the other long chain hybrid perovskites, such as $C_{10}CdCl$,[2] where the unit cell for the room-temperature phase **III** is monoclinic and the space group $P2_1/c$ ($a = 7.354(1)$, $b = 7.545(1)$, $c = 51.520(3)$ Å, $\beta = 91.74(1)^\circ$), which then transforms to an orthorhombic unit cell for phase **I**, space group *Amaa*, with no halving of the unit cell axis ($a = 7.460(2)$, $b = 7.546(2)$, $c = 54.64(2)$ Å).

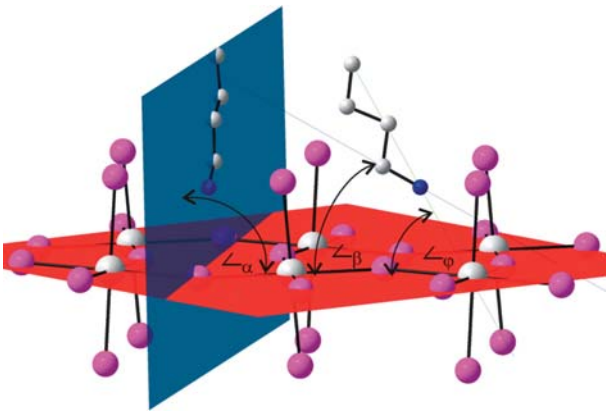

Fig. 5 The geometric quantities used for characterizing the cation orientation relative to the inorganic layers. The least-squares plane through the lead atoms is shown in red and the least squares plane through the C and N atoms of the alkylammonium cations is shown in blue.

To better describe the geometric changes that take place during the phase transitions, we introduced geometric quantities in a previous paper in which the phase changes of the related inorganic–organic layered perovskite-type hybrids with general formula $[(C_nH_{2n+1}NH_3)PbI_4]$ (n = 4, 5 and 6)[12] were investigated (see Fig. 5). These are the tilt angle φ, abbreviated $\angle_\varphi$, which corresponds to the angle between a plane through the inorganic layers (red plane in Fig. 5) and a vector connecting the first and last atom of each chain, for example the nitrogen atom N(1) and the carbon atom C(12) in the case of $C_{12}PbI$; the tilt of the plane angle $\angle_\alpha$ of the chains, which defines the dihedral angle between a plane containing all the atoms of the alkylammonium chains (blue plane in Fig. 5) and the lead atoms of the inorganic layers (red plane in Fig. 5); and the tilt angle $\angle_\beta$ of the ammonium group, which defines the angle between a vector connecting the atoms N(1) and C(1) and a plane through the lead atoms of the inorganic layers (red plane in Fig. 5).

The position of the ammonium group relative to the inorganic layer is affected by the phase changes and a procedure for describing its position is important as well as the effect this has on the hydrogen bonding configuration. The "box" within which the ammonium groups are positioned is defined by the four equatorial, or bridging iodides, and the four axial, or terminal iodides that protrude above the layer. In projection, the ammonium group is contained within a parallelogram defined by the four bridging iodides (depicted in green in Fig. 6). By projection onto this parallelogram, the ammonium group is found in proximity to either an acute or an obtuse angle of the parallelogram.

In theory, the ammonium group can hydrogen bond to any of these eight iodides mentioned above but it is found that the three hydrogens either bond to two terminal iodides and one bridging iodide (terminal halogen configuration) or to two bridging iodides and one terminal iodide (bridging halogen configuration). This classification is mentioned in the review by Mitzi.[13] All the compounds described here in their various phases adopt the terminal halogen configuration. However, there are two ways that the hydrogens can adopt the terminal or bridging halogen configuration: The three iodides to which the hydrogens bond

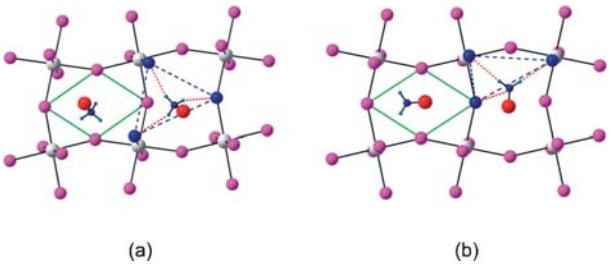

Fig. 6 The parallelogram defined by the four bridging iodides is shown in green and the right-angled and equilateral triangles are shown as dashed blue lines. (a) The obtuse angled position and the equilateral configuration. (b) The acute angled position and the right-angled configuration.

can be at the vertices of either an equilateral triangle or a right-angled triangle (depicted with dashed blue lines in Fig. 6). There is a correlation between the position of the ammonium group and the type of terminal halogen configuration: If the ammonium group is in the acute angled position, the ammonium group has the right-angled configuration of hydrogen bonds and the reverse case, if the ammonium group is in the obtuse angled position, the ammonium group has the equilateral configuration. The phase changes in $C_{12}PbI$, $C_{14}PbI$, $C_{16}PbI$ and $C_{18}PbI$ are as a result of the movement between these two geometries of their respective alkylammonium chains.

The corner-sharing PbI_6 octahedra that make up the 2-D layers are also affected by these phase changes. For the layered perovskite-type hybrids, two out of a three possible tilts[14] are encountered: a tilt perpendicular to the inorganic sheets (θ tilt), so that adjacent corner-shared octahedra are rotated relative to each other. The angle of the θ tilt is correlated with the bridging angle Pb–I–Pb, which deviates from 180°. The second kind of tilt is parallel to the layers (Ψ tilt), so that the layers are corrugated in one direction. The corrugation angle is measured by the angle between the normal to the inorganic layers and the vector connecting the Pb atom and the terminal I.

The orthorhombic phase III of $C_{16}PbI$ (3a)

Crystal packing. The crystal structure of the orthorhombic phase **III** of $C_{16}PbI$, **3a**, was determined at 293 K in the space group *Pbca*. Fig. 7(a) clearly shows a bidimensional arrangement in which two layers of interdigitated hexadecylammonium cations are embedded between two consecutive inorganic $[PbI_6]$ sheets, forming an alternating inorganic–organic layered structure. The unit cell contains three inorganic layers. The lead atoms are offset from layer to layer, resulting in a staggered arrangement of adjacent layers. The packing diagram of $C_{16}PbI$ in phase **III** is closely related to the K_2NiF_4 structure type, which too has corner-sharing layers of NiF_6 octahedra, that are staggered.[14] In the direction perpendicular to the layers, the organic ammonium cations hydrogen bond to the anionic inorganic layers *via* charge-assisted N–H···I hydrogen bonds. There are weak van der Waals forces between two adjacent organic ammonium chains (nearest neighbour distance is 4.162(1) Å).

The inorganic layer. The inorganic layer is built up from characteristic corner-sharing PbI_6 octahedra. The asymmetric

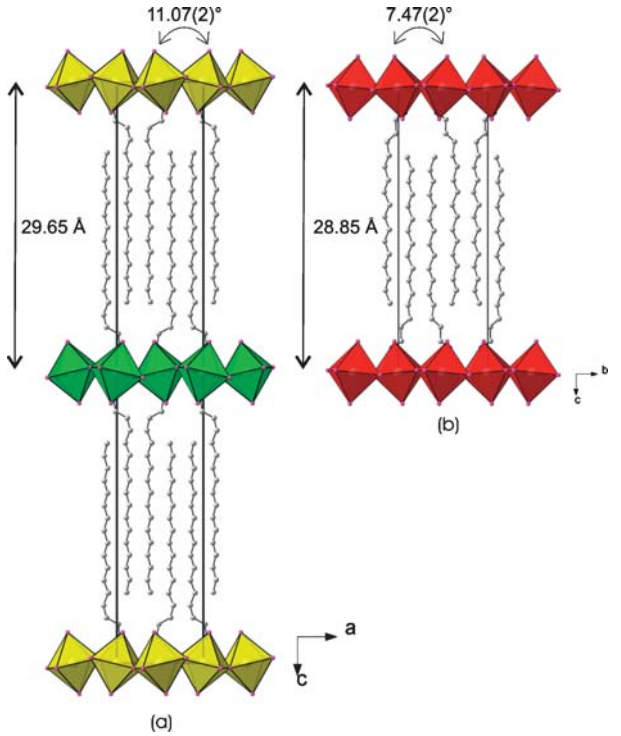

Fig. 7 The most striking feature of the phase transition is the change in crystal system from orthorhombic to monoclinic and the halving of the longest cell axis. (a) The orthorhombic phase **III** has successive inorganic layers staggered, shown in yellow and green. (b) The monoclinic phase **II** has eclipsed inorganic layers, shown in red.

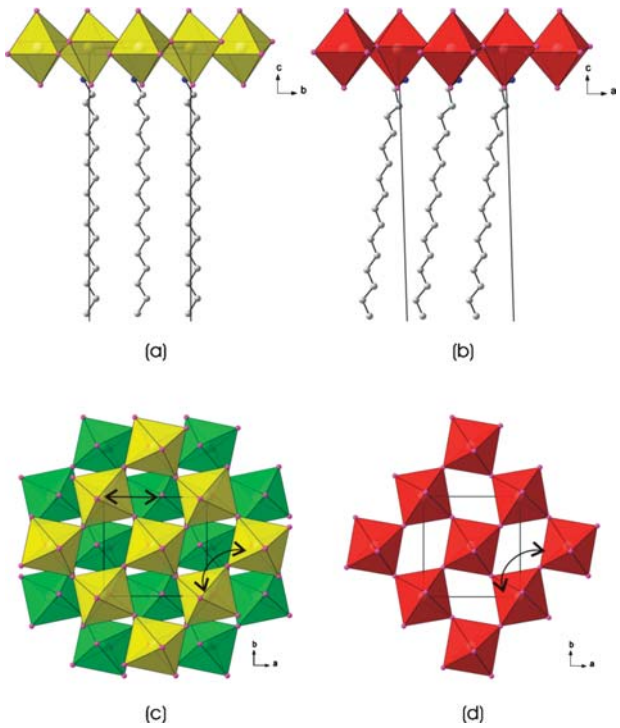

Fig. 8 The hexadecylammonium cation chain has a tilt angle of 3.9(1)° in the orthorhombic phase **III** (a), which increases to 9.7(1) in the monoclinic phase **II** (b). (c) A top view of phase **III**, illustrating the staggered layers in this phase and the direction of the offset. (d) The same top view of phase **II**, where every inorganic layer is eclipsed. The θ tilt is shown by the curved double-headed arrows.

unit consists of a lead atom on a special position and two iodide atoms, I(1) occupying the terminal position and I(2) occupying the bridging position in the layers. As shown in the projection perpendicular to the layers, along the *c*-axis, the PbI_6 octahedra are rotated by 149.52(3)° relative to each other (Fig. 8(c)). This rotation translates into a θ tilt = 30.48(3)°. Furthermore, the perovskite layers are corrugated in the *a*-direction by an angle of Ψ = 11.07(2)° with respect to the *ab*-plane. The coordination geometry around the Pb atom shows no axial compression of the octahedral geometry, with the bridging Pb(1)–I(2) distances shorter than the axial distances Pb(1)–I(1). The angle between *cis* related iodine atoms deviate from 90°, with all *trans* angles 180°.

The organic part and the intermolecular arrangement. The hexadecylammonium cation sits on a general position. The tilt of the chain relative to the inorganic layers is approximately $\angle_{\varphi}$ = 3.9(1)° (Fig. 8(a)). The chains are ordered within the organic layer and interdigitated up to the thirteenth carbon atom of the chain next to it. The plane of the chain is angled at $\angle_{\alpha}$ = 88.9(1)° to the inorganic layer. The chain has a torsion angle of 99(2)° between C(1)–C(2)–C(3)–C(4), with the remainder of the bonds within the chain in an all-*trans* planar configuration (Fig. 9(a)).

The inorganic–organic hydrogen bonds. The hydrogen bonds between the organic and inorganic entities adopt the terminal halogen configuration together with the equilateral configuration (See Table 2 and Fig. 9(c)). The hydrogen acceptor distances to the terminal halides I(1) are 2.77 and 2.96 Å and to the bridging halide I(2) 2.95 Å.

The monoclinic phase II of $C_{16}PbI$ (3b)

Crystal packing. The crystal structure of the monoclinic phase **II** of $C_{16}PbI$, **3b**, was determined at 341 K in the space group $P2_1/a$. Fig. 7(b) clearly shows a bidimensional arrangement in which two layers of interdigitated hexadecylammonium cations are embedded between two consecutive inorganic $[PbI_6]$ sheets, forming an alternating organic–inorganic layered structure. The unit cell contains two inorganic layers. The lead atoms are aligned from layer to layer, resulting in an eclipsed arrangement of adjacent layers, typical of monoclinic unit cells. The packing diagram of $C_{16}PbI$ in phase **II** is closely related to the $RbAlF_4$ structure type, which too has corner-sharing layers of AlF_6 octahedra, that are eclipsed.[14] In the direction perpendicular to the layers, the organic ammonium cations hydrogen bond to the anionic inorganic layers *via* charge-assisted N–H···I hydrogen bonds. There are weak van der Waals forces between two adjacent organic ammonium chains (nearest neighbour distance is 4.118(5) Å).

The inorganic layer. The inorganic layer is built up from characteristic corner-sharing PbI_6 octahedra. The asymmetric unit consists of a lead atom on a special position and two iodide atoms, I(1) occupying the terminal position and I(2) occupying the bridging position in the octahedra. The tilts of the PbI_6 octahedra are θ = 21.62(3)° around the *c*-axis and Ψ = 7.46(2)°

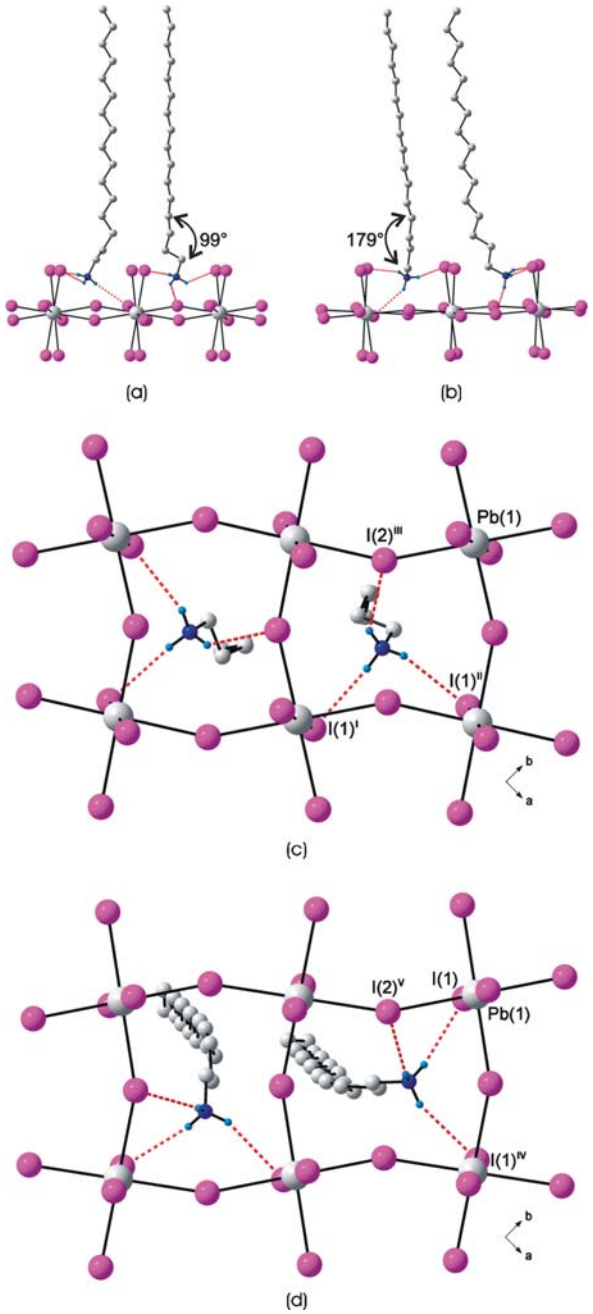

Fig. 9 The most significant variation in the hexadecylammonium chain of $C_{16}PbI$, is the change in the torsion angle around the C(2)–C(3) bond, (a) phase **III** and (b) phase **II**. As a consequence of the torsion angle change, the ammonium group changes its position relative to the inorganic layers from obtuse (c) to acute (d). Atoms labelled with superscripts (i), (ii), (iii), (iv) and (v) are at $(x, y - 1, z)$, $(-x + 5/2, y - 1/2, z)$, $(-x + 3/2, y - 1/2, z)$, $(x + 1/2, -y + 3/2, z)$ and $(-x + 3/2, y - 1/2, -z + 2)$, respectively.

along the *b*-axis. The coordination geometry around the Pb atom shows axial compression of the octahedral geometry, with the bridging Pb(1)–I(2) distances longer than the terminal distances Pb(1)–I(1). The angle between *cis* related iodine atoms deviate from 90°, with all *trans* angles 180°.

The organic part and the intermolecular arrangement. The hexadecylammonium cation sits on a general position. The tilt of the chain relative to the inorganic layers is approximately $\angle_{\varphi} = 9.7(1)^{\circ}$ (Fig. 8(b)). The chains are ordered within the inorganic layer and interdigitated up to the thirteenth carbon atom of the chain next to it. The plane of the chain is angled at $\angle_{\alpha} = 85.3(1)^{\circ}$ to the inorganic layer. The carbon atoms in the chain are in an all-*trans* planar conformation (Fig. 9(b)).

The inorganic–organic hydrogen bonds. The hydrogen bonds between the organic and inorganic entities adopt the terminal halogen configuration and the right-angled configuration (see Table 2 and Fig. 9(d)). The hydrogen acceptor distances to the terminal halides I(1) are 2.74 and 2.92 Å and to the bridging halide I(2) 3.01 Å.

Detail of the phase transition $C_{16}PbI$ phase III to $C_{16}PbI$ phase II

The crystal structures before and after the transitions were determined. There are two main conformational changes that occur at the phase transition at 340.0 K. The alkylammonium chain loses its + anti-clinal torsion angle around the C(2)–C(3) bond so that phase **II** has a planar zigzag arrangement of all the carbon atoms and the chain tilts so that it is no longer directly above the lead atoms. The second conformational change is a vertical shift of every middle inorganic layer in phase **III** by half a unit cell in the direction of the corrugation resulting in all the lead atoms being exactly above each other in phase **II**. Two adjacent layers now eclipse each other and subsequently the unit cell axis perpendicular to the layers halves. These two changes take place in a concerted fashion and are accompanied by other small geometric changes.

The inorganic layer and octahedra. Phase **III** has the lead atoms offset from each other when viewed down the long *c*-axis and the octahedra are corrugated in opposite directions, *i.e.* every other layer is corrugated in the same direction. Every second layer has lead atoms with the same fractional *x* and *y* coordinates. To get the lead atoms aligned down each layer, one has to translate every second layer by approximately half the *a*-unit cell axis in the direction of the *a*-axis. Fig. 8(c) shows the inorganic layers in phase **III** when viewed directly down the *c*-axis and the offset between the yellow and green coloured layers. Fig. 8(d) shows the same view for phase **II** down the *c*-axis and the lead atoms now have identical *x* and *y* fractional coordinates. After the phase transition from **III** to **II**, the degree of corrugation decreases for all the layers from $\Psi = 11.07(2)$ to $7.46(2)^{\circ}$.

In both phases **III** and **II**, the octahedra have three unique bond distances. Iodides that are *trans* related have the same bond distances and are exactly 180° opposed to each other by virtue of the inversion centre centred on the lead atom. In the orthorhombic phase **III**, the average bond length is $3.1838(121)^{\circ}$. The bond to the terminal halide I(1) the longest, is the same length above and below the octahedra. The two bond lengths to the bridging halide I(2) are shorter by 0.0152 and 0.0239 Å. The maximum deviation from 90° for a *cis* angle is $3.452(7)^{\circ}$. The degree of puckering of the octahedra as measured by the Pb(1)–I(2)–Pb(1) bridging angle is $149.52(3)^{\circ}$.

An increase in temperature leads to a more symmetrical geometry of the PbI_6 octahedra. The average bond length decreases slightly in the monoclinic phase **II** to 3.1825(30) Å

Table 2 Hydrogen bonding details of all compounds

D–H···A	D–H/Å	H···A/Å	D···A/Å	∠(D–H···A)/°	Symmetry transformation
1a, **III**					
N(1)–H(1A)···I(1)	0.89	2.93	3.591(15)	133	$-x + 5/2, y - 1/2, z$
N(1)–H(1B)···I(1)	0.89	2.76	3.648(14)	173	$x, y - 1, z$
N(1)–H(1C)···I(2)	0.89	2.97	3.704(14)	141	$-x + 3/2, y - 1/2, z$
1b, **II**					
N(1)–H(1A)···I(2)	0.89	3.13	3.765(9)	130	$-x + 3/2, y - 1/2, -z + 2$
N(1)–H(1B)···I(1)	0.89	2.72	3.800(8)	170	—
N(1)–H(1C)···I(1)	0.89	2.83	3.718(9)	172	$x + 1/2, -y + 3/2, z$
2a, **III**					
N(1)–H(1A)···I(1)	0.89	2.98	3.609(13)	130	$-x + 5/2, y - 1/2, z$
N(1)–H(1B)···I(1)	0.89	2.77	3.650(12)	170	$x, y - 1, z$
N(1)–H(1C)···I(2)	0.89	2.98	3.681(12)	137	$-x + 3/2, y - 1/2, z$
2b, **II**					
N(1)–H(1A)···I(2)	0.89	2.73	3.598(15)	165	$x + 1/2, -y + 3/2, z$
N(1)–H(1B)···I(1)	0.89	3.07	3.639(14)	124	—
N(1)–H(1C)···I(1)	0.89	2.95	3.720(18)	145	$x + 1/2, -y + 3/2, z$
3a, **III**					
N(1)–H(1A)···I(1)	0.89	2.96	3.594(12)	130	$-x + 5/2, y - 1/2, z$
N(1)–H(1B)···I(1)	0.89	2.77	3.651(11)	174	$x, y - 1, z$
N(1)–H(1C)···I(2)	0.89	2.95	3.674(12)	140	$-x + 3/2, y - 1/2, z$
3b, **II**					
N(1)–H(1A)···I(2)	0.89	3.01	3.796(11)	148	$-x + 3/2, y - 1/2, -z + 2$
N(1)–H(1B)···I(1)	0.89	2.74	3.567(10)	156	—
N(1)–H(1C)···I(1)	0.89	2.92	3.744(11)	156	$x + 1/2, -y + 3/2, z$
4a, **III**					
N(1)–H(1A)···I(1)	0.89	2.98	3.611(13)	129	$-x + 5/2, y - 1/2, z$
N(1)–H(1B)···I(1)	0.89	2.77	3.645(12)	167	$x, y - 1, z$
N(1)–H(1C)···I(2)	0.89	3.00	3.667(13)	133	$-x + 3/2, y - 1/2, z$
4b, **II**					
N(1)–H(1A)···I(2)	0.89	3.03	3.811(13)	148	$-x + 3/2, y - 1/2, -z + 2$
N(1)–H(1B)···I(1)	0.89	2.74	3.574(11)	156	—
N(1)–H(1C)···I(1)	0.89	2.97	3.784(12)	153	$x + 1/2, -y + 3/2, z$

but more significant is the decrease in the range of bond lengths to only 0.0055 Å. In the monoclinic phase, the longest bond length is no longer to the terminal halide but to one of the bridging halides (3.1859(8) Å) with the remaining two almost the same (Pb(1)–I(1): 3.1813(11) Å and Pb(1)–I(2): 3.1804(8) Å. The bond angles show a similar trend as before, with the *cis* angles now deviating at most by 2.49° from 90° and the bridging angle increasing to 158.40(2)°.

The alkylammonium chain and hydrogen bonding geometry. When the layers slide relative to each other, the hexadecylammonium cation chain is forced to change its orientation relative to the layers. Since the ammonium headgroup is anchored to the iodide atoms and the chains are interdigitated, the chains can accommodate the layer movement by tilting relative to the normal of the layers. The chains increase their tilt angle from $\angle_{\varphi} = 3.9(1)^\circ$ to 9.9(1)°.

The hexadecylammonium cation has a non-planar arrangement at room temperature and a planar arrangement in the higher temperature phase. The ammonium group is clearly bent out of the plane of the carbon atoms in phase **III** (Fig. 9(a)) and by rotating 80° around the C(2)–C(3) bond moves into the same plane as the carbon atoms in phase **II** (Fig. 9(b)). A consequence of the new arrangement of the chains between the layers is a reduction of the interlayer spacing by 0.8030 Å in going from the orthorhombic to the monoclinic phase.

In the orthorhombic phase **III**, the hexadecylammonium cation lies along the short diagonal of the parallelogram. The ammonium group occupies the obtuse position and adopts the equilateral configuration (Fig. 9(c)). When the compound is heated and undergoes the phase transition, the hexadecylammonium cation moves relative to the parallelogram from the obtuse angle to the acute angle. The hydrogen bonding scheme is now right-angled (Fig. 9(d)). The rotation in the torsion angle and the change in position of the ammonium group relative to the inorganic layer is reflected in the increase of the tilt angle $\angle_{\beta}$ of the ammonium head group. This angle doubles from 29.8(6)° to 61.0(7)°.

The transformations of C_{12}PbI and C_{18}PbI

The detailed analysis of the inorganic–organic layered perovskite-type structure of C_{16}PbI before and after the phase transition can be applied to the structures of C_{12}PbI and C_{18}PbI before and after their respective first phase transition, at 314.9 and 346.3 K, respectively. Table 3 summarizes the main geometrical features that were discussed in the previous section as they apply to C_{16}PbI. The same trends are observed in C_{12}PbI and C_{18}PbI.

The special case of C_{14}PbI

The phase transition from the orthorhombic phase **III** of C_{14}PbI, **2a**, to the monoclinic phase **II**, **2b**, is *via* single-crystal-to-single crystal as in C_{16}PbI. The previous papers did not investigate this compound.[9–11] The inorganic layer shifts as in the other three structures and the changes in the geometric parameters follow the same trends, shown in Table 3. However, when the phase transition occurs, the torsion angle changes only from 101(2)° between C(1)–C(2)–C(3)–C(4) to 105(4)° (see Fig. 10(a) and (b)). The ammonium group completes its movement from the obtuse position to the acute position as observed

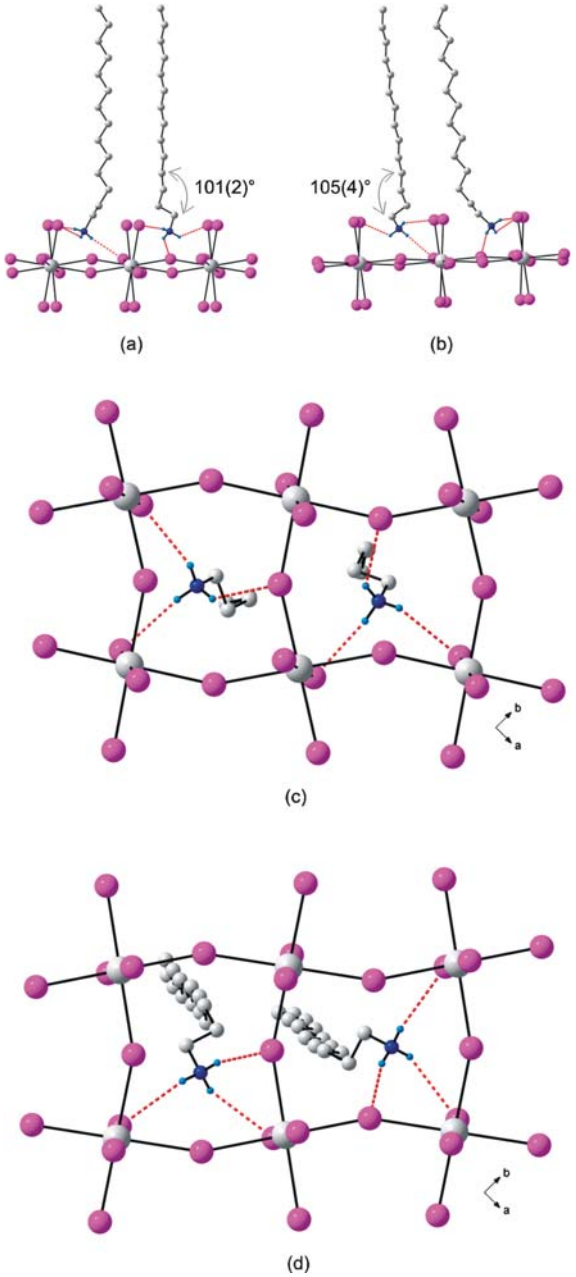

Fig. 10 (a) The orthorhombic phase **III** of $C_{14}PbI$, which is the same as the orthorhombic phases of all three other hybrids. (b) The monoclinic phase **II** of $C_{14}PbI$ is different from the other hybrids as the tetradecylammonium chain is not in an all-planar *trans* conformation. The ammonium group changes its position relative to the inorganic layers from obtuse (c) to acute (d).

in the other three hybrids but the conformational change around the C(2)–C(3) bond is negligible (see Fig. 10(c) and (d)). The reason for why the structure of phase **II** does not have the all-*trans* planar conformation could be due to the phase transition not going to completeness.

Conclusions

The compounds $[(C_nH_{2n+1}NH_3)_2PbI_4]$ (n = 12, 14, 16 and 18), which belong to the family of inorganic–organic layered perovskite-type hybrids, have two phase transitions above room temperature. The first or premelting transition from phase **III** to phase **II** has a much lower enthalpy than the second, melting transition, and has been the subject of this report. Accurate single-crystal structures of the phases of the hybrids before and after the first premelting transition shows that three major changes occur:

(i) the packing of the inorganic layers changes from staggered to eclipsed;

(ii) the position of the ammonium group changes relative from the layers from obtuse to acute, and

(iii) the conformation of the hydrocarbon chains changes around the C(2)–C(3) bond for $C_{12}PbI$, $C_{16}PbI$ and $C_{18}PbI$ ($C_{14}PbI$ remains the same).

All these processes take place concertedly and in almost identical fashion for the materials $C_{12}PbI$, $C_{16}PbI$ and $C_{18}PbI$. In the case of $C_{14}PbI$ the processes can be regarded as similar. It is important to note that particularly the room-temperature structures presented here as well as the proposed mechanism of the phase transition is markedly different from what has previously been proposed by Vasudevan, Seshadri and co-workers.[9–11] Their structural model was however inferred primarily from spectroscopic data, and as such can not be considered as conclusive as the structures and mechanism presented in this paper.

Experimental

Materials

All reagents and solvents employed were commercially available and used as received without further purification. Differential Scanning Calorimetry (DSC) data were collected on a Mettler Toledo 822^e at a scan rate of 5 K min^{-1} in sealed aluminium pans under air.

Synthesis

Preparation of $[(C_{12}H_{25}NH_3)_2PbI_4]$, 1. 0.048 g PbI_2 (0.104 mmol) was dissolved in 3 mL 47% HI in a sample vial. Thereafter, 0.030 g $C_{12}H_{25}NH_2$ (0.162 mmol) was added and the precipitate dissolved with a methanol (5 mL)–ethyl acetate (3 mL) mixture. The crystals were grown by slow evaporation over a number of days. A yellow single crystal suitable for X-ray diffraction analysis was selected and studied. Elemental analysis (%). Found: C 24.97, H 4.81, N 2.66. Calc. for $C_{24}H_{56}I_4N_2Pb$: C 26.51, H 5.19, N 2.58.

Preparation of $[(C_{14}H_{29}NH_3)_2PbI_4]$, 2. 0.015 g PbI_2 (0.104 mmol) was dissolved in 1 mL 47% HI in a sample vial. Thereafter, 0.010 g $C_{14}H_{29}NH_2$ (0.047 mmol) was added and the precipitate dissolved with 5 mL ethyl acetate. The crystals were grown by slow evaporation over a number of days. A yellow single crystal suitable for X-ray diffraction analysis was selected and studied. Elemental analysis (%). Found: C 30.16, H 5.74, N 2.46. Calc. for $C_{28}H_{64}I_4N_2Pb$: C 29.41, H 5.64, N 2.45.

Preparation of $[(C_{16}H_{33}NH_3)_2PbI_4]$, 3. 0.062 g PbI_2 (0.134 mmol) was dissolved in 1 mL 47% HI in a sample vial. Thereafter, 0.009 g $C_{16}H_{33}NH_2$ (0.037 mmol) was added and

Table 3 Geometric parameters for all compounds in their phases

Geometric parameter	**1a**, **III**	**1b**, **II**	**2a**, **III**	**2b**, **II**	**3a**, **III**	**3b**, **II**	**4a**, **III**	**4b**, **II**
Interlayer spacing/Å	24.51(9)	23.8647(16)	27.0781(7)	26.412(6)	29.6484(9)	28.846(8)	32.2236(11)	31.424(4)
Bridging angle Pb(1)–I(2)–Pb(1)/°	150.19(3)	157.42(2)	149.94(3)	158.43(4)	149.52(3)	158.40(3)	149.39(3)	158.83(2)
θ tilt/°	29.81(3)	22.58(2)	30.06(3)	21.57(4)	30.48(3)	21.60(3)	30.61(3)	21.17(2)
Corrugation or Ψ tilt/°	11.21(2)	6.86(1)	11.17(2)	7.34(2)	11.07(2)	7.47(2)	10.99(2)	7.70(1)
Tilt of chains $\angle_{\varphi}$/°	5.4(1)	12.0(1)	4.4(1)	10.7(1)	3.9(1)	9.7(1)	3.4(1)	8.8(1)
Tilt of plane $\angle_{\alpha}$/°	88.8(1)	85.1(1)	89.0(1)	85.0(1)	88.9(1)	85.3(1)	89.1(1)	85.5(1)
Tilt of NH_3 group $\angle_{\beta}$/°	31.0(9)	61.3(6)	31.4(9)	48.8(9)	29.8(6)	61.0(7)	32.7(8)	59.6(7)
Position of ammonium group	Obtuse	Acute	Obtuse	Acute	Obtuse	Acute	Obtuse	Acute
Hydrogen bonding configuration	Equilateral	Right-angled	Equilateral	Right-angled	Equilateral	Right-angled	Equilateral	Right-angled
Torsion angle C(1)–C(2)–C(3)–C(4)/°	97(2)	179(2)	101(2)	105(4)	99(2)	179(2)	115(2)	172(2)

the precipitate dissolved with 8 mL ethyl acetate. The crystals were grown by slow evaporation over a number of days. A yellow single crystal suitable for X-ray diffraction analysis was selected and studied. Elemental analysis (%). Found: C 32.38, H 5.91, N 2.40. Calc. for $C_{32}H_{72}I_4N_2Pb$: C 32.04, H 6.05, N 2.34.

Preparation of $[(C_{18}H_{37}NH_3)_2PbI_4]$, 4. 0.033 g PbI_2 (0.072 mmol) was dissolved in 1 mL 47% HI in a sample vial. Thereafter, 0.008 g $C_{18}H_{37}NH_2$ (0.030 mmol) was added and the precipitate dissolved with 15 mL ethyl acetate. The crystals were grown by slow evaporation over a number of days. A yellow

Table 4 Crystal data for compounds **1a**, **1b**, **2a**, **2b**, **3a**, **3b**, **4a** and **4b**

	1a, **III**	**1b**, **II**	**2a**, **III**	**2b**, **II**
Formula	$(C_{12}H_{25}NH_3)_2[PbI_4]$	$(C_{12}H_{25}NH_3)_2[PbI_4]$	$(C_{14}H_{29}NH_3)_2[PbI_4]$	$(C_{14}H_{29}NH_3)_2[PbI_4]$
M_r	1087.50	1087.50	1143.60	1143.60
T/K	293	319	293	335
Crystal size/mm	0.44 × 0.37 × 0.02	0.40 × 0.18 × 0.02	0.44 × 0.30 × 0.01	0.44 × 0.30 × 0.01
Crystal system	Orthorhombic	Monoclinic	Orthorhombic	Monoclinic
Space group (no.)	*Pbca* (61)	$P2_1/a$ (14)	*Pbca* (61)	$P2_1/a$ (14)
a/Å	8.8645(2)	8.6882(6)	8.8474(1)	8.6774(16)
b/Å	8.5149(1)	9.0031(6)	8.5167(1)	9.0143(19)
c/Å	49.0253(9)	23.8647(16)	54.1561(7)	26.412(6)
β/°	90	92.487(2)	90	92.492(13)
V/Å^3	3700.45(12)	1854.4(2)	4080.70(8)	2064.0(7)
Z	4	2	4	2
D_c/g cm^{-3}	1.952	1.937	1.861	1.840
μ(Mo-Kα)/mm^{-1}	7.909	7.849	7.177	7.095
θ range/°	1.66–25.50	1.71–25.50	0.75–25.50	1.54–25.50
Total reflections	30177	14752	25519	19105
No. unique data (R_{int})	3430 (0.0631)	3469 (0.0491)	3803 (0.0510)	3840 (0.0669)
No. data with $I \geq 2\sigma(I)$	2820	2597	3005	2675
$R1$	0.0551	0.0348	0.0540	0.0531
$wR2$ (all data)	0.1362	0.0998	0.1147	0.1586
	3a, **III**	**3b**, **II**	**4a**, **III**	**4b**, **II**
Formula	$(C_{16}H_{33}NH_3)_2[PbI_4]$	$(C_{16}H_{33}NH_3)_2[PbI_4]$	$(C_{18}H_{37}NH_3)_2[PbI_4]$	$(C_{18}H_{37}NH_3)_2[PbI_4]$
M_r	1199.71	1199.71	1255.81	1255.81
T/K	293	341	293	348
Crystal size/mm	0.36 × 0.17 × 0.03	0.36 × 0.17 × 0.03	0.48 × 0.27 × 0.01	0.40 × 0.12 × 0.01
Crystal system	Orthorhombic	Monoclinic	Orthorhombic	Monoclinic
Space group (no.)	*Pbca* (61)	$P2_1/a$ (14)	*Pbca* (61)	$P2_1/a$ (14)
a/Å	8.8167(1)	8.673(2)	8.7825(1)	8.6917(9)
b/Å	8.5222(1)	9.012(3)	8.5401(1)	9.0456(10)
c/Å	59.2906(9)	28.846(8)	64.4472(11)	31.424(4)
β/°	90	91.816(6)	90	91.586(8)
V/Å^3	4454.96(10)	2253.4(11)	4833.76(11)	2469.7(5)
Z	4	2	4	2
D_c/g cm^{-3}	1.789	1.768	1.726	1.689
μ(Mo-Kα)/mm^{-1}	6.579	6.503	6.068	5.938
θ range/°	2.06–25.50	2.12–25.50	1.26–25.50	1.30–25.50
Total reflections	22340	19104	21829	21316
No. unique data (R_{int})	4147 (0.0405)	4199 (0.0755)	4500 (0.0754)	4594 (0.0646)
No. data with $I \geq 2\sigma(I)$	3256	2937	3430	2621
$R1$	0.0519	0.0400	0.0556	0.0412
$wR2$ (all data)	0.1292	0.1170	0.1346	0.1085

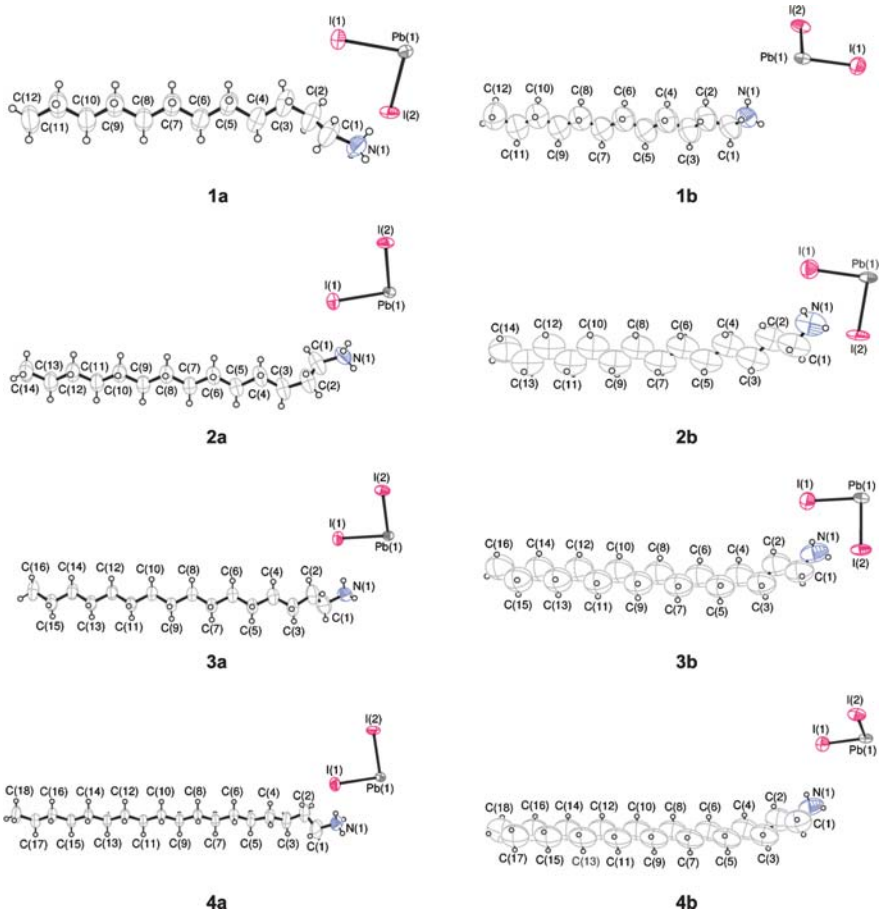

Fig. 11 The asymmetric unit and atomic numbering scheme of the four compounds **1–4**. The phase **III** structures are shown in the left column and are labelled **1a–4a**, and the corresponding phase **II** structures are shown on the right, labelled **1b–4b**. The anisotropic displacement parameters are drawn at the 50% probability level.

single crystal suitable for X-ray diffraction analysis were selected and studied. Elemental analysis (%). Found: C 34.71, H 6.11, N 2.24. Calc. for $C_{36}H_{80}I_4N_2Pb$: C 34.43, H 6.42, N 2.23.

X-Ray crystallography

All diffraction data were collected on a Bruker Apex II CCD diffractometer[15] with graphite-monochromated Mo-Kα radiation (λ = 0.71073) at room temperature and at high temperature using a Oxford Cryostream 700. Data reduction and cell refinement were done using SAINT-NT[16] and space groups of these compounds were determined from systematic absences by *XPREP*[16] and further justified by the refinement results. Face indexed absorption corrections were performed on all crystals using *XPREP*.[16] In all cases, the structures were solved in the *WinGx*[17] Suite by direct methods using *SHELXS97*[18] and refined using full-matrix least squares/difference Fourier techniques using *SHELXL97*.[18] All non-hydrogen atoms were refined with anisotropic displacement parameters. After that, all hydrogen atoms were placed at idealized positions and refined as riding atoms with the relative isotropic parameters of the heavy atoms to which the are attached. The H atoms on the N atom are placed in idealized positions, staggered with respect to the shortest other bond to the atom to which the NH_3^+ is attached. This optimizes the hydrogen bonding contacts.

In all reported crystal structures, the fractional coordinates of the Pb atom in the asymmetric unit were chosen to be at the special position (1,1,1). This aids in the comparison of related structures. The crystal structures **1b**, **2b**, **3b** and **4b**, that crystallized in a monoclinic system, were refined in the non-standard setting $P2_1/a$ of space group $P2_1/c$ so that a direct comparison among cell dimensions is possible when compared to the crystal structures of **1a**, **2a**, **3a** and **4a**.

The C–C carbon distances in all structures whose intensity data were collected at room and higher temperatures, do not have normal carbon distances as a result of thermal motion of the carbon chains. All carbon distances were then restrained in SHELX to reasonable molecular geometries and the anisotropic displacement parameters restrained to be equal in the direction of the bonds.

Diagrams and publication material were generated using *ORTEP*,[19] *PLATON*[20] and *DIAMOND*.[21] Experimental details of the X-Ray analyses are provided in Table 4. The atomic numbering scheme and anisotropic displacement parameters are shown in Fig. 11.

Acknowledgements

The University of the Witwatersrand and the National Research Fund (GUN 2069064) are thanked for the award of a

research grant and for providing the infrastructure required to do this work. A. L. is grateful to Prof. G. Heger for his valuable comments and interest in this work.

References

1 S. Kammoun, M. Kamoun, A. Daoud and F. Romain, *Phys. Status Solidi A*, 1996, **156**, 317.
2 R. Kind, S. Pleško, H. Arend, R. Blinc, B. Žekš, J. Seliger, B. Ložar, J. Slak, A. Levstik, C. Filipič, V. Žagar, G. Lahajnar, F. Milla and G. Chapuis, *J. Chem. Phys*., 1979, **71**, 2118.
3 M. R. Ciajolo, P. Corradini and V. Pavone, *Gazz. Chim. Ital*., 1976, **106**, 807.
4 M. Koželj, V. Rutar, I. Zupančič, R. Blinc, H. Arend, R. Kind and G. Chapuis, *J. Chem. Phys*., 1981, **74**, 4123.
5 S. S. Nagapetyan, Yu. I. Dolzhenko, E. R. Arakelova, V. M. Koshkin, Yu. T. Struchkov and V. E. Shklover, *Russ. J. Inorg. Chem*., 1988, **33**, 2806.
6 (*a*) K. W. Lee, C. H. Lee and C. E. Lee, *Phys. Rev. B*, 2003, **67**, 134424-1; (*b*) K. W. Lee and C. E. Lee, *Solid State Commun*., 2003, **126**, 343; (*c*) C. Carfagna, M. Vacatello and P. Corradini, *Gazz. Chim. Ital*., 1977, **107**, 131; (*d*) E. Landi, V. Salerno and M. Vacatello, *Gazz. Chim. Ital*., 1977, **107**, 27; (*e*) V. Busico, V. Salerno and M. Vacatello, *Gazz. Chim. Ital*., 1979, **109**, 581; (*f*) M. Vacatello and P. Corradini, *Gazz. Chim. Ital*., 1974, **104**, 773; (*g*) M. Vacatello and P. Corradini, *Gazz. Chim. Ital*., 1973, **103**, 1027; (*h*) M. Vacatello, M. De Girolamo and V. Busico, *J. Chem. Soc., Faraday Trans*., 1981, **77**, 2367; (*i*) C. Almirante, G. Minoni and G. Zerbi, *J. Phys. Chem*., 1986, **90**, 852; (*j*) G. F. Needham, R. D. Willett and H. F. Franzen, *J. Phys. Chem*., 1984, **88**, 674; (*k*) M. A. Arriandiaga, M. J. Tello, J. Fernandez, H. Arend and J. Roos, *Phys. Status Solidi A*, 1978, **48**, 53.
7 T. Ishihara, J. Takahashi and T. Goto, *Phys. Rev. B*, 1990, **42**, 11099.
8 D. G. Billing and A. Lemmerer, unpublished results.
9 S. Barman, N. V. Venkataraman, S. Vasudevan and R. Seshadri, *J. Phys. Chem. B*, 2003, **107**, 1875.
10 N. V. Venkataraman, S. Bhagyalakshmi, S. Vasudevan and R. Seshadri, *Phys. Chem. Chem. Phys*., 2002, **4**, 4533.
11 N. V. Venkataraman, S. Barman, S. Vasudevan and R. Seshadri, *Chem. Phys. Lett*., 2002, **358**, 139.
12 D. G. Billing and A. Lemmerer, *Acta Crystallogr., Sect. B*, 2007, **63**, 735–747.
13 D. B. Mitzi, *Prog. Inorg. Chem*., 1999, **48**, 1.
14 (*a*) D. M. Hatch, H. T. Stokes, K. S. Aleksandrov and S. V. Miguel, *Phys. Rev. B*, 1989, **39**, 9282; (*b*) D. M. Hatch and H. T. Stokes, *Phys. Rev. B*, 1987, **35**, 8509.
15 *Bruker 2005*, *APEX2*, Version 1.0-27, Bruker AXS Inc., Madison, Wisconsin, USA.
16 *Bruker 2004*, *SAINT-PLUS*, Version 7.12 (including *XPREP*), Bruker AXS Inc., Madison, Wisconsin, USA.
17 L. J. Farrugia, *J. Appl. Crystallogr*., 1997, **30**, 565.
18 G. M. Sheldrick, *SHELX, release 97-2 (includes SHELXS and SHELXL)*, University of Göttingen, 1997.
19 L. J. Farrugia, WinGX, *J. Appl. Crystallogr*., 1999, **32**, 837.
20 A. L. Spek, *J. Appl. Crystallogr*., 2003, **36**, 7.
21 K. Brandenburg, *Diamond*, Version 2.1e., Crystal Impact GbR, Bonn, Germany.

